INORGANIC CHEMISTRY FRONTIERS

RESEARCH ARTICLE

View Article Online
View Journal | View Issue

Cite this: *Inorg. Chem. Front.*, 2026, **13**, 726

Amino-imidazolin-2-imine Cu(I) complexes: ligand screening and tuning of photophysical properties

Leo Wessel, †[a] Oliver Lange, †[b] Lars E. Burmeister, [b] Lars Denker,[a] Michael Karnahl, *[b] Stefanie Tschierlei, *[b] Matthias Tamm *[a] and René Frank *[a]

Amino-imidazolin-2-imines (HAmIm) are introduced as a new class of strong monoanionic N,N′-chelating ligands for Cu(I) complexes. The reaction of HAmIm with CuCl, followed by deprotonation to give AmIm$^-$, affords the dinuclear precursor [Cu_2(μ-AmIm)$_2$], which serves as a versatile platform for the synthesis of structurally diverse mononuclear Cu(I) complexes. Coordination with diimine ligands (phenanthroline or neocuproine) yields distorted tetrahedral [Cu(AmIm)(diimine)] species featuring a broad UV/vis absorption. In contrast, reaction with monodentate phosphines (**L_1**–**L_5**) affords trigonal planar complexes [Cu(AmIm)(L)], which are non-emissive in solution, but exhibit pronounced emission in the solid state. All ten new complexes were structurally characterised by single-crystal X-ray diffraction, enabling a direct correlation between coordination geometry and photophysical properties. Photophysical studies and TDDFT calculations reveal fluorescence in the nanosecond-range originating from ligand-to-ligand and mixed metal–ligand-to-ligand charge-transfer transitions (LL′CT, mMLL′CT). The emission properties correlate with the nature of the phosphine ligand. In particular, complexes containing chalcogen-bridged phosphines (**L_4** and **L_5**) display the highest intensities and lifetimes of up to ≈29.2 and ≈13.9 ns, respectively. Temperature-dependent time-resolved measurements confirm prompt fluorescence and exclude thermally activated delayed fluorescence (TADF), underscoring the intrinsic nature of the emission. These results highlight the modular potential of HAmIm ligands to access structurally diverse and photoactive Cu(I) complexes with tunable solid-state emission.

Received 21st August 2025,
Accepted 12th November 2025

DOI: 10.1039/d5qi01753j

rsc.li/frontiers-inorganic

Introduction

The interest in photocatalysts and photosensitisers arises from their ability to harvest (solar) light and convert it into chemical reactivity.[1,2] Transition metal complexes have received considerable attention in this field, particularly those based on Ru(II) (4d) [3–6] and Ir(III) (5d).[7–9] Their inherently strong spin–orbit coupling (SOC) facilitates efficient intersystem crossing, enabling access to long-lived triplet states. However, the scarcity and high cost of these noble metals has stimulated the search for Earth-abundant alternatives, especially those with 3d transition metals.[10–12]

Among these, photoactive Cu(I) complexes have been explored in a wide range of applications, including photoredox catalysis, solar fuel production, dye-sensitised solar cells, and light-emitting diodes.[13,14] Their closed-shell d^{10} configuration avoids low-lying metal-centred (MC) states, which are often responsible for rapid non-radiative deactivation in open-shell 3d systems. However, several excited-state deactivation processes in Cu(I) complexes, most notably due to geometric distortion upon excitation, remain a significant challenge.[15–17]

The coordination chemistry of Cu(I) spans two- to four-coordinate geometries. While four-coordinate, tetrahedral Cu(I) complexes are most extensively studied, they are prone to pseudo-Jahn–Teller flattening distortion towards square planar in the metal-to-ligand charge transfer (MLCT) excited state.[18–22] This distortion promotes non-radiative decay processes, limiting emission efficiency.[23,24] As a result, lower coordination numbers, particularly two- and three-coordinate Cu(I) complexes have come into focus. While two-coordinate Cu(I) complexes remain rare due to their high reactivity,[25–28] a growing number of more stable three-coordinate Cu(I) complexes have been reported over the past decade.[29–41]

In such systems, trigonal planar geometries can be stabilised by appropriate ligand design. Although DFT studies have shown that excited-state distortion towards T-shaped geome-

[a]*Institut für Anorganische und Analytische Chemie, Technische Universität Braunschweig, Hagenring 30, 38106 Braunschweig, Germany. E-mail: r.frank@tu-bs.de, m.tamm@tu-bs.de*
[b]*Department of Energy Conversion, Institute of Physical and Theoretical Chemistry, Technische Universität Braunschweig, Rebenring 31, 38106 Braunschweig, Germany. E-mail: michael.karnahl@tu-bs.de, s.tschierlei@tu-bs.de*
† Shared first authorship. Both authors contributed equally.

tries may occur,[29] suitable N,N′-chelating ligands in combination with sterically demanding ancillary ligands have been shown to enforce a rigid, luminescent three-coordinate structure.[30–32] The majority of examples are cationic or neutral complexes of the type $[Cu(NHC)(N,N')]^{+/0}$ (NHC = N-heterocyclic carbene; N,N′ = neutral or anionic bidentate nitrogen donor ligand such as bipyridines or pyrazolylpyridines).[30–41] Despite their low coordination number, many of these complexes display good stability and appreciable excited-state lifetimes.

Among the ligand systems applied in this context, amidines (HAm) and guanidines (HGu, see structures **A** in Fig. 1) as well as β-diketimines (HNacNac, see **B**) have found wide application as monoanionic N,N′-chelating ligands.[42–45] Upon deprotonation, they form four- or six-membered chelate rings with Cu(I), leading to photoactive complexes of types **E** and **F** (Fig. 1). For example, amidinate and guanidinate Cu(I) complexes (see **E**) have been combined with cyclic (alkyl)(amino)carbenes (CAACs) and have been proposed as white-luminescent emitters.[42]

More recently, three-coordinate β-diketiminate Cu(I) complexes (see **F** in Fig. 1) with phosphine or isonitrile co-ligands have been reported.[43–45] These systems still rely on six-membered chelates. Ligand scaffolds that enable stable five-membered N,N′-chelating Cu(I) complexes remain scarce. To address this gap, we have recently introduced amino-imidazolin-2-imines (HAmIm, **C**) as a new class of monoanionic N,N′-chelating ligands.[46,47] These ligands incorporate an imidazolin-2-imine scaffold (see **D**), which acts as a strong nitrogen-based σ- and π-donor, as illustrated by the resonance structures (**D** in Fig. 1). Derivatives of **D** have previously been used as ancillary ligands in various metal complexes.[48–62] The superior behaviour of HAmIm (see **C**) *vs.* β-diketimine ligands was recently demonstrated in several examples of main group chemistry.[63,64] Thus, the complete series of boraketones of the type X═B(AmIm) (X = O, S, Se, Te) could only be prepared with HAmIm ligands, while previous approaches employing β-diketimine ligands failed.[46] In a second example, the group 13 carbenoids E(AmIm), E = Ga, In, Tl were found to be stronger donors compared to the related β-diketiminate analogues.[63] A detailed investigation traced these advantages to much better σ- and π-donor quality of $AmIm^-$ *vs.* β-diketiminate ligands. Moreover, $AmIm^-$ ligands have shown superior performance compared to β-diketiminate ligands in related cobalt and iron complexes.[65,66]

Building on these findings, we now report the synthesis and characterisation of the first Cu(I) complexes featuring HAmIm ligands. Their structural and photophysical properties were systematically studied as a function of the coordinated ancillary ligand.

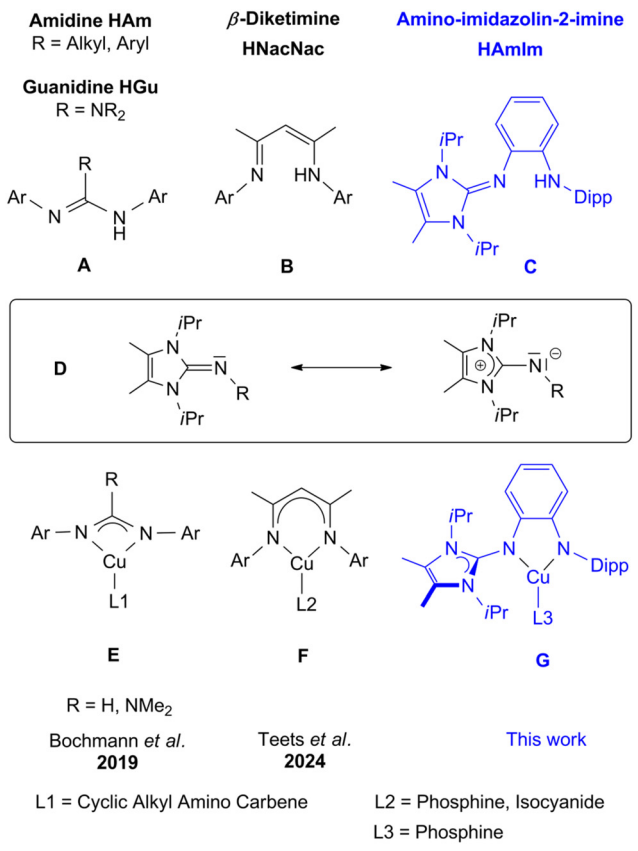

Fig. 1 Amidines and guanidines **A** and β-diketimines **B** give rise to monoanionic ligands in four- or six-membered photoactive Cu(I) complexes **E**, **F**. In a new approach amino-imidazolin-2-imine ligands **C** are employed to produce five-membered chelate complexes of type **G**. Ar = aryl group, Dipp = 2,6-diisopropylphenyl.

Results and discussion

Synthetic procedures and crystallography

The reaction of the neutral HAmIm ligand **C** with copper(I) chloride afforded complex **1**, [Cu(HAmIm)Cl], as a colourless material (Fig. 2). Coordination of ligand **C** is confirmed by the characteristic low-field shifts of all signals in the ^{1}H NMR spectrum (Fig. S1 and S2) as well as by X-ray crystallography (Fig. 2). In complex **1**, the imidazolin-2-imine entity (N1, see Fig. 2, bottom left) is a significantly stronger donor than the amine part (N4), which is corroborated by (i) the comparison of bond lengths Cu1–N1 [1.912(3) Å] < Cu1–N4 [2.495(3) Å], and (ii) the angle N1–Cu1–Cl1 [161.17(9)°] approaching linearity (Table 1).

The treatment of complex **1** with potassium bis(trimethylsilyl)amide, $K[N(SiMe_3)_2]$, caused a formal elimination of hydrogen chloride, resulting in the formation of the dinuclear, centrosymmetric complex **2**, $[Cu_2(\mu\text{-AmIm})_2]$ (Fig. 2, top right). In this complex, ligand **C** adopts its monoanionic form and bridges two Cu(I) ions, as verified by X-ray crystallography. While the bond length between the metal and the imine entity Cu1′–N1 [1.878(1) Å] in **2** is only slightly shorter than in its parent complex **1** [*d*(Cu1–N1) = 1.912(3) Å], the Cu1–N4 bond in **2** is significantly shorter than in **1** [*cf.* 2.495(3) Å in **1** *vs.* 1.8586(1) Å in **2**], reflecting its amide character. The formation of dinuclear complexes with linear geometry at Cu(I) is well documented for amidine (HAm)[67–70] and guanidine (HGu)[71,72]

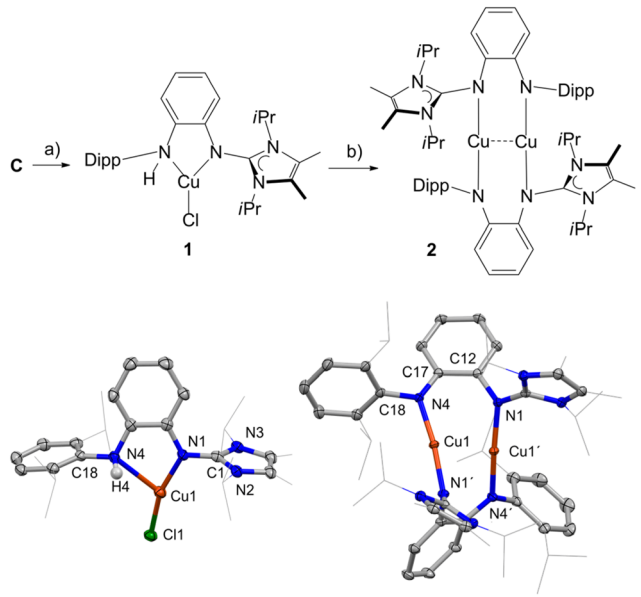

Fig. 2 Reagents and conditions: (a) 1.0 eq. CuCl, THF, 3 h, 10 °C, 89%. (b) 1.0 eq. K[N(SiMe$_3$)$_2$], THF, 30 h, 10 °C, 88%. Bottom left: molecular structure of complex **1**. Toluene and hydrogen atoms (except for N4–H4) are omitted. Selected bond distances [Å] and angles [°]: Cu1–N1 1.912(3), Cu1–N4 2.495(3), Cu1–Cl1 2.1272(9), N4–Cu1–N1 74.7(1), N1–Cu1–Cl1 161.17(9), N4–Cu1 –Cl1 123.46(7), σ = 359.27(5)°. Bottom right: molecular structure of complex **2**, which is located on a centre of inversion. Hydrogen atoms are omitted. Selected bond distances [Å] and angles [°]: Cu1–Cu1′ 2.4841(3), Cu1′–N1 1.878(1), Cu1–N4 1.8586(1), N1–Cu1–N4′ 173.10(5).

ligands. In contrast, Cu(I)-β-diketiminate complexes tend to be mononuclear, even with weak ligands such as ethylene, benzene, or toluene.[73,74] The distance between the copper centres Cu1–Cu1′ [2.4841(3) Å] in **2** compares well with reported values of related dinuclear complexes and suggests a weak contact interaction rather than strong bonding.[67–72] Thus, in the typical amidinate complex [Cu$_2$(Dipp-NCHN-Dipp)$_2$], the copper–copper distance was found to be 2.5420(7) Å.[69] Complex **2** is internally twisted, as indicated by the dihedral angle of N1–N4–N1′–N4′ of 55.7(3)°.

However, the ^{1}H NMR spectrum of compound **2** in solution (THF-D$_8$) reveals a highly symmetric behaviour, evident from the symmetry-related diagnostic signals of the aryl and nitrogen bound isopropyl groups (Fig. S3 and S4). Complex **2** is sensitive towards air and moisture, which required careful purification of all added ancillary ligands (see below). This sensitivity is illustrated by the reaction of complex **2** with a stoichiometric amount of degassed water, *i.e.* 1 eq. of water per copper atom (Fig. 3). This reaction resulted in the dinuclear complex [Cu(AmIm)$_2$(μ-OH)$_2$] (**3**), in which each copper centre is chelated by the monoanionic form AmIm$^-$ of ligand **C** and is bridged by hydroxido ligands. Compound **3** is centrosymmetric, with the copper centre adopting a square planar coordination geometry. The metrical parameters of compound **3** closely resemble those reported for similar neutral complexes with β-diketimine ligands,[75,76] or dicationic complexes with ethylene-bridged bis(imidazolin-2-imine) ligands.[52]

The reaction essentially involves an oxidation of Cu(I) in **2** to Cu(II) in **3**. Complex **3** gives rise to narrow lines in the ^{1}H NMR spectra, which can be attributed to the antiferromagnetic superexchange coupling between the two Cu(II) centres *via* the bridging hydroxido ligands (Fig. S5). ^{1}H NMR spectroscopy has emerged a useful tool for dinuclear copper(II) complexes with antiferromagnetic exchange coupling, *i.e.* values of $J < 0$.[77–80] In particular, strongly negative antiferromagnetic coupling constants of $J < 1000$ cm^{-1} give rise to almost diamagnetic

Table 1 Selected bond lengths (Å), bond angles (°) and the sum of the bond angles σ (°) for the complexes **4–10**. σ denotes the sum of all three bond angles N1–Cu1–N4, N1–Cu1–P1 and N4–Cu1–P1 encircling the central Cu1 atom. Experimental data from the crystal structure is denoted as "Xray", while computed structures are denoted as "DFT"

Tetrahedral complexes (coordination number = 4)

	Method	Cu1–N1	Cu1–N4	Cu1–N5	Cu1–N6	N1–Cu1–N4	N5–Cu1–N6	N1–Cu1–N6	N4–Cu1–N5
4	X-ray	2.0570(17)	1.9562(16)	2.0166(18)	2.2346(18)	83.53(7)	78.13(7)	121.45(7)	138.26(7)
	DFT	2.055	1.969	2.217	2.002	82.925	79.042	131.710	121.360
5	X-ray	2.0675(10)	1.9612(10)	1.9536(10)	2.3009(10)	83.23(4)	78.61(4)	103.50(4)	139.28(4)
	DFT	2.069	1.974	1.982	2.285	82.504	78.275	107.590	138.751

Trigonal planar complexes (coordination number = 3)

#	Method	Cu1–N1	Cu1–N4	Cu1–P1	N1–Cu–N4	N1–Cu P1	N4–Cu–P1	σ
6	X-ray	2.004(3)	1.930(3)	2.1313(11)	84.34(14)	135.50(10)	140.16(10)	359.98(7)
	DFT	2.021	1.941	2.152	84.1	133.1	142.2	359.4
7	X-ray	1.9867(7)	1.9426(7)	2.1325(2)	84.66(3)	139.46(2)	135.64(2)	359.77(1)
	DFT	2.013	1.949	2.149	83.942	137.664	138.062	359.7
8	X-ray	1.9948(19)	1.9322(19)	2.1298(6)	84.58(8)	136.59(6)	138.52(6)	359.69(4)
	DFT	2.013	1.952	2.158	83.611	137.691	138.329	359.6
9	X-ray	1.985(2)	1.925(2)	2.1185(7)	84.82(9)	135.49(6)	139.68(7)	360.00(4)
	DFT	2.009	1.941	2.147	84.299	136.786	138.406	359.5
10	X-ray	1.9879(9)	1.9283(9)	2.1276(3)	84.73(4)	134.98(3)	140.26(3)	359.97(2)
	DFT	2.018	1.952	2.157	83.991	135.563	140.415	360.0

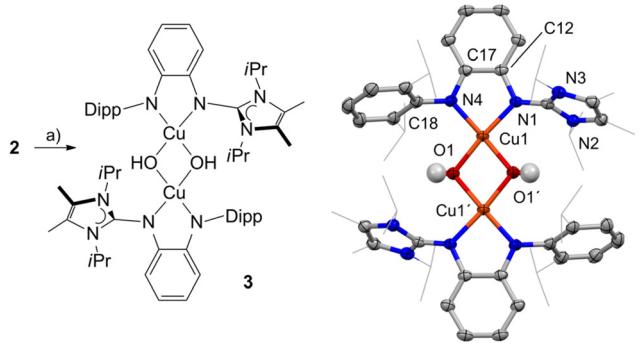

Fig. 3 Reagents and conditions: (a) 2.0 eq. degassed H_2O, THF, overnight, rt, 68%. Molecular structure of complex **3**, which has a centre of inversion. Benzene and hydrogen atoms (except for O–H) are omitted. Selected bond distances [Å] and angles [°]: Cu1–N1 1.9515(11), Cu1–N4 1.9153(12), Cu1–O1 1.9215(11), Cu1–Cu1′ 3.0271(4), N1–Cu1–O1′ 98.54 (5), N4–Cu1–O1 100.76(5), O1–Cu1–O1′ 76.54(6), N1–Cu1–N4 84.44(5), Cu1–O1–Cu1′ 103.45(6).

behaviour.[81] The presence of the bridging hydroxido ligand is corroborated by a broad singlet in the ^{1}H NMR spectrum at 1.77 ppm, as well as by an intense band in the IR spectrum at 3356 cm^{-1} (Fig. S6). Complex **2**, [Cu$_2$(μ-AmIm)$_2$], proved to be an ideal starting material for the synthesis of mononuclear Cu(I) complexes with tunable photophysical properties, induced by the addition of suitable ancillary ligands (Fig. 4). The bidentate ligands phenanthroline (phen) and neocuproine (neo) were employed first due to their known behaviour as electron acceptors. Reaction of complex **2** with the (carefully pre-dried) diimine ligands afforded [Cu(AmIm)(phen)] (**4**) and [Cu(AmIm)(neo)] (**5**), respectively. Compounds **4** and **5** were isolated as deep green crystalline solids.

In contrast to complex **3**, the oxidation state of +1 is retained in **4** and **5**, which is also reflected by the shorter Cu1–N1 and Cu1–N4 bond lengths in **3** compared to **4** and **5**. The geometrical data (Table 1) for the tetrahedral environment at copper in **4** and **5** compare well with those of similar heteroleptic Cu(I) β-diketiminate complexes containing the same diimine ligands.[82–84] However, while the reported β-diketiminate complexes display symmetric coordination of the β-diketiminate ligand with equal Cu–N bond distances, the AmIm$^-$ ligand shows pronounced asymmetric behaviour, as indicated by strongly unequal bond distances, *i.e.* Cu1–N1 = 2.057(2) Å *vs.* Cu1–N4 = 1.966(2) Å in **4** and Cu1–N1 = 2.068(1) Å *vs.* Cu1–N4 = 1.961(1) Å in **5**. Density functional theory (DFT) calculations further support this asymmetric binding mode (Table 1).

For both complexes **4** and **5**, the phen and neo ligands exhibit a profoundly asymmetric coordination behaviour with markedly tilted orientations. This is reflected in the unequal bond distances Cu1–N5 [2.017(2) Å in **4**, 1.954(1) Å in **5**] *vs.* Cu1–N6 [2.235(2) Å in **4**, 2.301(1) Å in **5**], as also validated by DFT calculations. However, the distorted alignment is absent in solution, as the ^{1}H NMR spectra of complexes **4** and **5** (Fig. S7–10) exhibit patterns characteristic of C_s-symmetry.

Beyond the bidentate ligands (phen and neo), monodentate phosphine ligands have recently been reported as ancillary ligands in photoactive three-coordinate β-diketiminate Cu(I) complexes.[45] Accordingly, complex **2** was reacted with a series of different phosphine ligands **L1–L5**, yielding the Cu(I) complexes **6–10** (Fig. 5). Orange-red crystals of **6–10**, suitable for X-ray crystallography (Table 1) were obtained. Complexes **6–10** display a distorted trigonal planar Y-geometry, as indicated by the sum of the three bond angles at the Cu(I) centre, which is close to 360° in each case (Fig. 6).

The ^{31}P{^{1}H} NMR spectra of complexes **6–10** show a significant downfield shift of the observed singlets compared to the uncoordinated ligands **L1–L5** (Fig. S12, S14, S16, S18 *vs.* S21, S24, S26, S28, S30). Although the solid-state structures of complexes **6–10** suggest C_1-symmetry, the ^{1}H NMR spectra (Fig. S19–S30) display a local C_s-symmetry for the AmIm$^-$ ligand. This suggests a certain degree of conformational flexi-

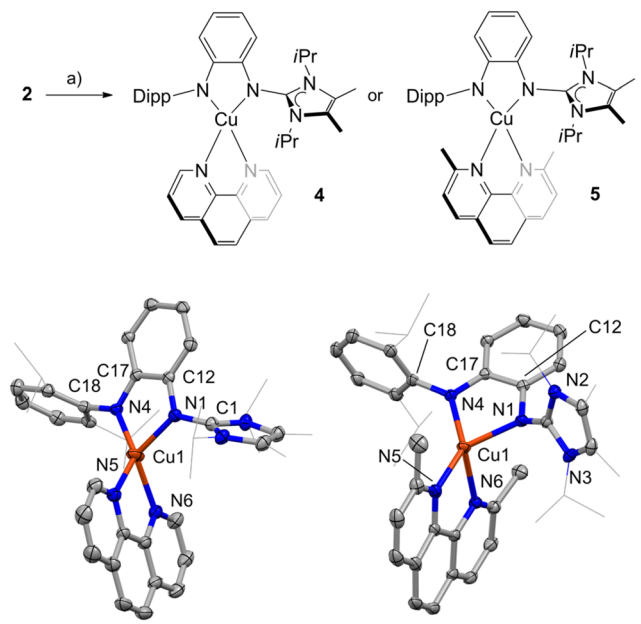

Fig. 4 Reagents and conditions: (a) 2.0 eq. phen or neo, THF, 48 h, 10 °C, 63% (**4**), 62% (**5**). Bottom: molecular structure of complex **4** (left) and **5** (right). Hydrogen atoms are omitted.

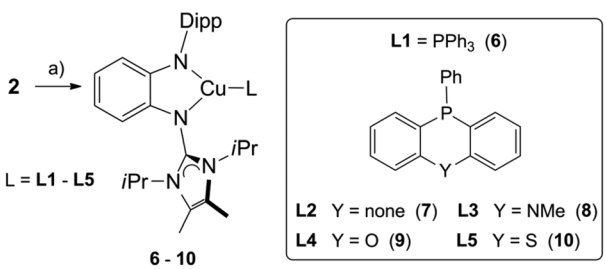

Fig. 5 Synthetic approach to complexes **6–10**. Reagents and conditions: (a) 2.0 eq. **L1–L5**, benzene, overnight, 10 °C, 89% (**6**), 90% (**7**), 74% (**8**), 60% (**9**), 60% (**10**).

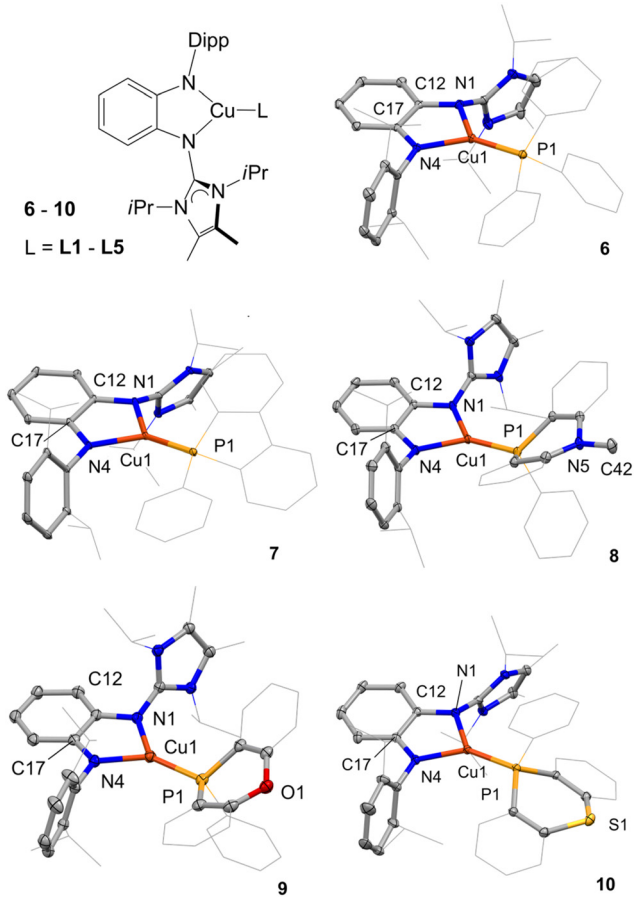

Fig. 6 Molecular structures of the complexes **6–10**. Hydrogen atoms and co-crystallised solvent are omitted for clarity.

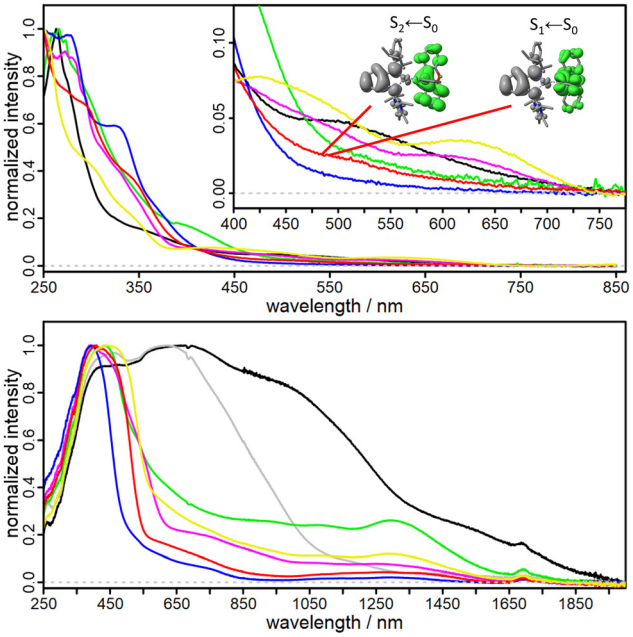

Fig. 7 Top: normalised absorption spectra of the complexes **4** (black), **5** (grey), **6** (green), **7** (pink), **8** (blue), **9** (red) and **10** (yellow) in inert tetrahydrofuran solution directly after preparation. The inset focuses on the visible region and displays the low-lying ligand-to-ligand charge transfer transitions of **9** through electron difference density plots (gain in green, loss in grey) using PBE0/def2-TZVP. Bottom: normalised solid-state KBr pellet absorption after preparation of the complexes **4–10** *vs.* pure KBr reference measured in diffuse reflectance mode.

bility for complexes **6–10** in solution, including planarisation at the N1 nitrogen atom as well as rotation around the Cu1–P1 bond axis. In contrast to the air-sensitive starting material **2**, solid samples of complexes **6–10** remain stable in moist air for at least 24 h, as indicated by their persistent colour and reproducible ^{1}H NMR spectra prior to air exposure. This behaviour is in contrast to related β-diketiminate copper complexes, which are reported to decompose at such conditions.[45]

Absorption and emission spectroscopy

Due to the intense colouration of the complexes **4–10**, their photophysical properties were investigated both in tetrahydrofuran solution and in the solid state (13 mm KBr pellets, <1.5 wt%), using a combination of spectroscopic and computational methods.

In inert tetrahydrofuran solution, all complexes exhibit one (**8**, **9**) or two (**4**, **7**, **10**) weak absorption bands in the visible region (>380 nm; Fig. 7, top). These bands are not observed in related β-diketiminate-Cu(I) systems bearing monodentate phosphine ligands, but absorption bands at the UV/vis edge are.[45] The absorption of **4** in tetrahydrofuran solution does not compare to other tetrahedral Cu(I) complexes bearing a phentype and β-diketiminate ligand, which have been reported to have panchromatic absorption covering the entire visible spectral region in solution.[76,82,83] TDDFT calculations (Fig. S32, S34, S36, S38, S40, S42, and S44) assign the visible bands to the $S_{1,2} \leftarrow S_0$ transitions of predominantly ligand-to-ligand charge transfer (LL′CT) character with minor metal-to-ligand charge transfer (MLCT) contributions. This excitation type is comparable to that in known β-diketiminate systems, but is slightly shifted towards LL′CT character.[2,45,82–84]

The charge transfer involves the highest occupied molecular orbital (HOMO) and the two lowest unoccupied molecular orbitals (LUMO and LUMO+1) (Fig. S31, S33, S35, S37, S39, S41, and S43). Similar to β-diketiminate systems, the HOMO is primarily localised on the five-membered $AmIm^{-}$ chelate ring and the phenyl backbone, and remains nearly isoenergetic within the same coordination type (Fig. 8).[2,45,82–84]

In contrast, the LUMOs are strongly influenced by the nature of the ancillary ligands, as reflected by the computed orbital energies (Fig. 8). However, spectral assignment is complicated due to (i) slight spectral changes upon dissolution, likely caused by tetrahydrofuran coordination, formation of coordination isomers, or reaction with traces of moisture (Fig. S45, S48, S51, S54, S57, and S60), (ii) the small oscillator strengths (Tables S6 and S12), and (iii) features, *i.e.* double-bands, observed for **7** and **10**, are not reproduced by TDDFT. For **4** and **5**, TDDFT overestimates the LL′CT bands (>690 nm, Fig. S32 and S34), suggesting that the experimentally observed

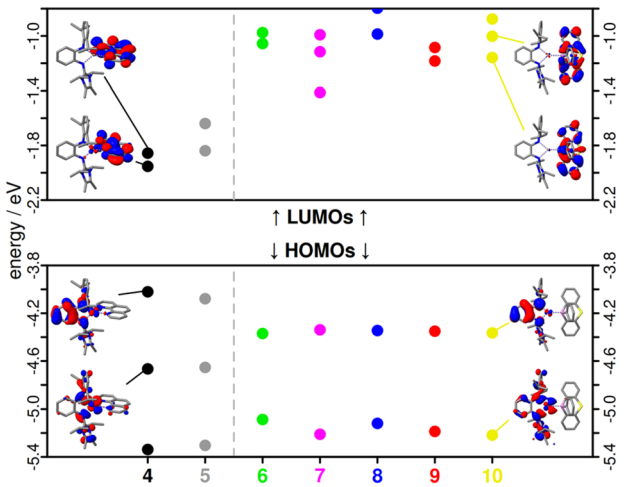

Fig. 8 Absolute molecular orbital energies in eV for the four-coordinate compounds **4** (black), **5** (gray) left and the three-coordinate compounds **6** (green), **7** (pink), **8** (blue), **9** (red) and **10** (yellow) using PBE0/def2-TZVP. The energies of the highest occupied molecular orbitals (bottom) and lowest unoccupied molecular orbitals (top) are shown. Molecular orbitals for **4** (left) and **10** (right) depict relevant and representative HOMOs and LUMOs for the tetrahedral and trigonal planar complexes.

visible bands may instead arise from more intense mixed metal–ligand-to-ligand charge transfer (mMLL′CT) transitions ($S_{3,4} \leftarrow S_0$, 544.7 to 603.6 nm), involving the HOMO−1 with contributions from the Cu atom, the imidazolin-2-imine, and amine regions. In contrast, the mMLL′CT excitations in **6–10** are outside the visible range (≈350 nm) and overlap with local $AmIm^-$-based transitions. No emission in tetrahydrofuran solution was detected upon excitation at 400 nm for **4** and **7–10**. Related trigonal planar and tetrahedral Cu(I) complexes bearing a β-diketiminate were also reported to be weakly phosphorescent to non-emissive in toluene solution.[43,45,76]

In contrast, the solid-state absorption spectra of KBr pellets (<1.5 wt%) are significantly broader and extend into the NIR region (Fig. 7, bottom; Fig. S46, S47, S49, S52, S55, S58, and S61). Complexes **4** and **5** display very broad absorptions with maxima at 660 and 626 nm, respectively, while **6–10** show three characteristic bands centred at ≈400 nm, ≈750–850 nm, and ≈1320 nm.

Upon excitation at 400 nm, only the trigonal planar complexes **6–10** exhibit solid-state luminescence (Fig. 9; Fig. S46, S47, S49, S52, S55, S58, and S61), with **9** (578 nm) and **10** (587 nm) emitting strongly and visibly to the naked eye. Emission from **6** (560 nm), **7** (623 nm), and **8** (556 nm) is considerably weaker under identical conditions. Notably, despite their broad absorption, complexes **4** and **5** have no emission in the solid state.

Time-resolved emission measurements using a femtosecond laser coupled to a streak camera system revealed biexponential decays in the nanosecond regime, with two components (Table 2 and Fig. S50, S53, S56, S59, S62). Comparable complexes in toluene solution display longer lifetimes in the

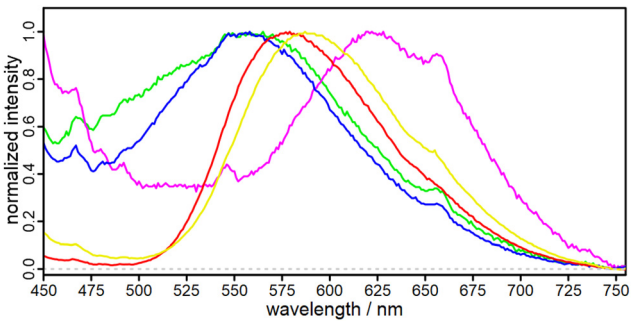

Fig. 9 Normalised uncorrected emission spectra of the complexes **6** (green), **7** (pink), **8** (blue), **9** (red), **10** (yellow) as KBr pellets excited at 400 nm.

microsecond range.[45] Both lifetimes are notably longer in **9** and **10**; **7** and **8** are similar, while **6** is significantly shorter. Both lifetimes τ_1 and τ_2 of **7–10** obtained *via* global lifetime analysis have strongly overlapping decay-associated spectra whose peak wavelengths λ_1 and λ_2 are negligibly shifted compared to each other (<10.4 nm). Only **6** shows a clear separation of 59 nm in its decay-associated spectra peak maxima (Fig. S50).

As the negligible peak wavelength shift of **7–10** could indicate thermally activated delayed fluorescence (TADF), an exemplary temperature-dependent emission study was conducted for complex **9** (Fig. S63). First, the emission intensity increases with lower temperature, and no spectral shift can be observed, which potentially excludes phosphorescence. The time scales of both components are identical under inert and ambient conditions (Fig. S59 and S63) and support prompt fluorescence with τ_1 fluctuating between 1 and 10 ns and τ_2 increasing slightly from 22 to 262 ns between 350 and 80 K. Furthermore, the log–log plot of emission intensity *vs.* time indicates no typical bend, which would separate the prompt and delayed fluorescence regime.[85–87] For that reason, TADF is potentially excluded, and both components are likely prompt fluorescence in the solid state.

In summary, all complexes display weak LL′CT and mMLL′CT absorptions in solution and are non-emissive under these conditions. In the solid state, the absorption bands shift and broaden, especially for the tetrahedral complexes **4** and **5**.

Table 2 Emissive lifetimes τ_1 and τ_2 in ns of compounds **6–10** determined *via* global lifetime analysis with a multiexponential sum fit model. The wavelengths λ_1 and λ_2 correspond to the fitted maxima of the amplitude A_i distribution of lifetime τ_i in the decay-associated spectrum (for more details: SI general information, time-resolved emission spectroscopy, Fig. S50, S53, S56, S59, and S62.)

Complex	τ_1/ns	λ_1/nm	τ_2/ns	λ_2/nm
6	0.17	523.8	1.03	582.8
7	0.47	657.2	10.1	665.6
8	0.59	563.4	10.5	573.8
9	1.49	607.1	29.2	602.5
10	0.97	591.7	13.9	591.9

However, only the trigonal planar complexes **6–10** exhibit fluorescence with biexponential decays and nanosecond lifetimes. The emission wavelengths correlate well with the computed HOMO–LUMO gaps: complex **7** has the smallest gap and longest emission wavelength, followed by **9** and **10**, and finally **6** and **8** (Fig. 8 and Table 2).

Chalcogen-bridged phosphine ligands (complexes **9** and **10**) have significantly enhanced emission intensity and prolonged excited-state lifetimes, followed by the methylated amino-bridged derivative (complex **8**), and by the system with no bridge atom (complex **7**). In contrast, complex **6** with unbridged phosphine **L1** exhibits the weakest emission and shortest lifetimes.

Electrochemical behaviour

The redox properties of the complexes **7–10** were investigated by cyclic voltammetry in inert tetrahydrofuran solution (Table 3, Fig. S64). Complexes **4–6** could not be reliably measured due to the rapid changes observed that occurred upon dissolution, as discussed above. As a reference, the individual ligands (Fig. 5, right) were analysed separately; while the ligand **L2** is redox-inactive within the accessible solvent window, **L3–L5** exhibit irreversible oxidation events at +0.40 V, +0.70 V, and +0.72 V *vs.* Fc/Fc^+, respectively. In contrast, the neutral HAmIm ligand **C** exhibits two irreversible oxidation processes at +0.31 and +0.64 V, as well as one irreversible reduction at −0.73 V, which becomes prominent after the oxidation cycle.

The complexes **7–10** each display a single irreversible oxidation in the narrow potential range of +0.10 to +0.18 V, independent of the specific phosphine ligand. The close agreement with the oxidation potentials of the uncoordinated HAmIm ligand, along with the small variation in computed HOMO energies (Fig. 8), suggests that this oxidation is centred on the coordinated $AmIm^-$ ligand. This behaviour is similar to earlier reports on β-diketiminate Cu(I) complexes, where the oxidation has been described as a mixed event involving both the Cu(I)/Cu(II) couple and the anionic ligand.[45,82–84]

A reversible reduction process is observed for all complexes **7–10** between −0.72 V and −0.77 V. DFT calculations of **7–10** predict the LUMO, *i.e.* the electron-accepting orbital, to be located on the respective phosphine ligand. This prediction is comparable with β-diketiminate systems, where reductive events are typically located on the neutral diimine or phosphine co-ligands.[45,82–84] However, no reduction associated with the uncoordinated phosphine ligands is detected within the accessible potential window (Fig. S64), which makes an assignment of the reduction from the electrochemical experiments difficult.

Table 3 Oxidation (E_{ox}) and reduction potentials (E_{red}) of the complexes **7–10**. Potentials are referenced against the ferrocene/ferrocenium (Fc/Fc^+) couple

Complex	E_{ox}/V *vs.* Fc/Fc^+	E_{red}/V *vs.* Fc/Fc^+
7	0.10^i	-0.75^r
8	0.13^i	-0.77^r
9	0.16^i	-0.72^r
10	0.18^i	-0.76^r

[i]Since the oxidation is irreversible the potential of maximum current is given. [r]For the reversible reduction events the half-step potential ($E_{1/2}$) is given

Conclusions

In this work, a modular family of Cu(I) complexes bearing amino-imidazolin-2-imine (HAmIm) ligands was developed and systematically investigated. Upon deprotonation, $AmIm^-$ acts as a monoanionic N,N′-chelating ligand with strong σ- and π-donor characteristics, coordinating to Cu(I) centres in various structural motifs. A total of ten new copper complexes were synthesised and all structurally characterised by single-crystal X-ray diffraction, highlighting the robustness and versatility of the HAmIm ligand framework. The dinuclear complex $[Cu_2(\mu\text{-}AmIm)_2]$ served as a versatile precursor for both tetrahedral [Cu(AmIm)(diimine)] and trigonal planar [Cu(AmIm)(phosphine)] species. The ability to access both coordination motifs from a single precursor underlines the modularity of the ligand system and sets a benchmark within Cu(I) coordination chemistry.

TDDFT calculations and spectroscopic studies revealed that the HOMO is consistently located on the five-membered $AmIm^-$ chelate ring and phenyl backbone, while the HOMO−1 involves the central Cu atom, the imidazoline-2-imine moiety, and the amine region. In contrast, the low-lying LUMOs are defined by the neutral donor ligand. This electronic arrangement offers a rational design principle, as the excitation type (LL′CT *vs.* mMLL′CT) and transition energies can be selectively tuned by varying the ancillary ligand.

Notably, the tetrahedral complexes **4** and **5** exhibit broad absorption bands in the visible to near-infrared region, yet remain non-emissive. In contrast, the trigonal planar phosphine complexes **6–10** display solid-state fluorescence with nanosecond-range lifetimes and biexponential decay profiles. This distinct separation between absorber- and emitter-type complexes demonstrates how coordination geometry dictates photophysical behaviour and thus possible applications.

Among them, complexes **9** and **10**, bearing chalcogen-bridged phosphines, show the strongest luminescence, correlating with enhanced HOMO–LUMO separation and extended excited-state lifetimes (≈29 ns). These properties position them as promising candidates for OLEDs or sensing applications. Temperature-dependent time-resolved emission studies confirm the presence of prompt fluorescence and rule out thermally activated delayed fluorescence (TADF). The absence of TADF simplifies the excited-state landscape and points to genuine ligand-controlled fluorescence.

Electrochemical measurements indicate that the irreversible oxidation agrees with computational data and is traced to the $AmIm^-$ ligand. While the computational data suggests the phosphine ligands to be the site of reduction, an assignment

of the electrochemical experiments remains ambiguous. This finding is comparable to six-membered β-diketiminate systems and highlights the potential modularity of these new Cu(I) systems.

This study introduces the HAmIm ligand family and establishes design principles for tuning the absorption and emission profiles of Cu(I) complexes. By expanding the N,N′-chelating ligand repertoire, HAmIm ligands open new avenues for the design of photoactive materials. Future studies will include further variations of the ligands, with a particular focus on isonitriles and cyclic (alkyl)(amino)carbenes (CAACs), given the recently reported benefits of such ligands in photoactive copper complexes.[88]

Conflicts of interest

There are no conflicts to declare.

Data availability

The data supporting this article are included in the supplementary information (SI). Supplementary information: additional experimental, synthetic, computational, spectroscopic, and electrochemical details. See DOI: **https://doi.org/10.1039/d5qi01753j**.

CCDC 2428671–2428680 (**1–10**) contain the supplementary crystallographic data for this paper.[89a–j]

Acknowledgements

We would like to thank Johannes P. Zurwellen for his help with the temperature-dependent time-resolved emission measurements. L. E. B. thanks the German Federal Environmental Foundation for financial support (DBU, AZ: 20024/029). Funded by the Deutsche Forschungsgemeinschaft (DFG, German Research Foundation) – Project Number 524554621.

References

1 L. Wang, Recent Advances in Metal-Based Molecular Photosensitizers for Artificial Photosynthesis, *Catalysts*, 2022, **12**, 919.
2 D. Kim, V. Q. Dang and T. S. Teets, Improved transition metal photosensitizers to drive advances in photocatalysis, *Chem. Sci.*, 2024, **15**, 77–94.
3 D. A. Nicewicz and D. W. C. MacMillan, Merging Photoredox Catalysis with Organocatalysis: The Direct Asymmetric Alkylation of Aldehydes, *Science*, 2008, **322**, 77–80.
4 J. M. R. Narayanam, J. W. Tucker and C. R. J. Stephenson, Electron-Transfer Photoredox Catalysis: Development of a Tin-Free Reductive Dehalogenation Reaction, *J. Am. Chem. Soc.*, 2009, **131**, 8756–8757.
5 M. A. Ischay, M. E. Anzovino, J. Du and T. P. Yoon, Efficient Visible Light Photocatalysis of [2 + 2] Enone Cycloadditions, *J. Am. Chem. Soc.*, 2008, **130**, 12886–12887.
6 S. Cerfontaine, S. A. M. Wehlin, B. Elias and L. Troian-Gautier, Photostable Polynuclear Ruthenium(II) Photosensitizers Competent for Dehalogenation Photoredox Catalysis at 590 nm, *J. Am. Chem. Soc.*, 2020, **142**, 5549–5555.
7 E. D. Nacsa and D. W. C. MacMillan, Spin-Center Shift-Enabled Direct Enantioselective α-Benzylation of Aldehydes with Alcohols, *J. Am. Chem. Soc.*, 2018, **140**, 3322–3330.
8 J.-H. Shon, D. Kim, M. D. Rathnayake, S. Sittel, J. Weaver and T. S. Teets, Photoredox catalysis on unactivated substrates with strongly reducing iridium photosensitizers, *Chem. Sci.*, 2021, **12**, 4069–4078.
9 V. Q. Dang and T. S. Teets, Reductive photoredox transformations of carbonyl derivatives enabled by strongly reducing photosensitizers, *Chem. Sci.*, 2023, **14**, 9526–9532.
10 H. Takeda, Y. Monma and O. Ishitani, Highly Functional Dinuclear CuI-Complex Photosensitizers for Photocatalytic CO_2 Reduction, *ACS Catal.*, 2021, **11**, 11973–11984.
11 A. Aydogan, R. E. Bangle, A. Cadranel, M. D. Turlington, D. T. Conroy, E. Cauët, M. L. Singleton, G. J. Meyer, R. N. Sampaio, B. Elias and L. Troian-Gautier, Accessing Photoredox Transformations with an Iron(III) Photosensitizer and Green Light, *J. Am. Chem. Soc.*, 2021, **143**, 15661–15673.
12 L. A. Büldt and O. S. Wenger, Chromium(0), Molybdenum (0), and Tungsten(0) Isocyanide Complexes as Luminophores and Photosensitizers with Long-Lived Excited States, *Angew. Chem., Int. Ed.*, 2017, **56**, 5676–5682.
13 M. J. Leitl, D. M. Zink, A. Schinabeck, T. Baumann, D. Volz and H. Yersin, Copper(I) Complexes for Thermally Activated Delayed Fluorescence: From Photophysical to Device Properties, *Top. Curr. Chem.*, 2016, **374**, 25.
14 C. E. Housecroft and E. C. Constable, TADF: Enabling luminescent copper(I) coordination compounds for light-emitting electrochemical cells, *J. Mater. Chem. C*, 2022, **10**, 4456–4482.
15 J. K. McCusker, Electronic structure in the transition metal block and its implications for light harvesting, *Science*, 2019, **363**, 484–488.
16 C. Förster and K. Heinze, Photophysics and photochemistry with Earth-abundant metals – fundamentals and concepts, *Chem. Soc. Rev.*, 2020, **49**, 1057–1070.
17 C. Wegeberg and O. S. Wenger, Luminescent First-Row Transition Metal Complexes, *JACS Au*, 2021, **1**, 1860–1876.
18 M. W. Mara, K. A. Fransted and L. X. Chen, Interplays of excited state structures and dynamics in copper(I) diimine complexes: Implications and perspectives, *Coord. Chem. Rev.*, 2015, **282–283**, 2–18.
19 M. Iwamura, S. Takeuchi and T. Tahara, Ultrafast Excited-State Dynamics of Copper(I) Complexes, *Acc. Chem. Res.*, 2015, **48**, 782–791.
20 F. Doettinger, Y. Yang, M. Karnahl and S. Tschierlei, Bichromophoric Photosensitizers: How and Where to

Attach Pyrene Moieties to Phenanthroline to Generate Copper(I) Complexes, *Inorg. Chem.*, 2023, **62**, 8166–8178.
21 M. Rentschler, P. J. Boden, M. A. Argüello Cordero, S. T. Steiger, M.-A. Schmid, Y. Yang, G. Niedner-Schatteburg, M. Karnahl, S. Lochbrunner and S. Tschierlei, Unexpected Boost in Activity of a Cu(I) Photosensitizer by Stabilizing a Transient Excited State, *Inorg. Chem*, 2022, 61, 12249–12261.
22 M. A. Argüello Cordero, P. J. Boden, M. Rentschler, P. Di Martino-Fumo, W. Frey, Y. Yang, M. Gerhards, M. Karnahl, S. Lochbrunner and S. Tschierlei, Comprehensive Picture of the Excited State Dynamics of Cu(I)- and Ru(II)-Based Photosensitizers with Long-Lived Triplet States, *Inorg. Chem.*, 2022, **61**, 214–226.
23 L. X. Chen, G. Jennings, T. Liu, D. J. Gosztola, J. P. Hessler, D. V. Scaltrito and G. J. Meyer, Rapid Excited-State Structural Reorganization Captured by Pulsed X-rays, *J. Am. Chem. Soc.*, 2002, **124**, 10861–10867.
24 L. X. Chen, G. B. Shaw, I. Novozhilova, T. Liu, G. Jennings, K. Attenkofer, G. J. Meyer and P. Coppens, MLCT State Structure and Dynamics of a Copper(I) Diimine Complex Characterized by Pump–Probe X-ray and Laser Spectroscopies and DFT Calculations, *J. Am. Chem. Soc.*, 2003, **125**, 7022–7034.
25 D. Di, A. S. Romanov, L. Yang, J. M. Richter, J. P. H. Rivett, S. Jones, T. H. Thomas, M. A. Jalebi, R. H. Friend, M. Linnolahti, M. Bochmann and D. Credgington, High-performance light-emitting diodes based on carbene-metal-amides, *Science*, 2017, **356**, 159–163.
26 R. Hamze, J. L. Peltier, D. Sylvinson, M. Jung, J. Cardenas, R. Haiges, M. Soleilhavoup, R. Jazzar, P. I. Djurovich, G. Bertrand and M. E. Thompson, Eliminating nonradiative decay in Cu(I) emitters: >99% quantum efficiency and microsecond lifetime, *Science*, 2019, **363**, 601–606.
27 P. Schmeinck, D. Sretenović, J. Guhl, R. Kühnemuth, C. A. M. Seidel, C. M. Marian, M. Suta and C. Ganter, Luminescent Copper(I)-Complexes with an Anionic NHC obtained via a Coordination Polymer as Versatile Precursor, *Eur. J. Inorg. Chem.*, 2023, **26**, e202300416.
28 J. Föller, C. Ganter, A. Steffen and C. M. Marian, Computer-Aided Design of Luminescent Linear N-Heterocyclic Carbene Copper(I) Pyridine Complexes, *Inorg. Chem.*, 2019, **58**, 5446–5456.
29 K. A. Barakat, T. R. Cundari and M. A. Omary, Jahn–Teller Distortion in the Phosphorescent Excited State of Three-Coordinate Au(I) Phosphine Complexes, *J. Am. Chem. Soc.*, 2003, **125**, 14228–14229.
30 K. Lee, P. N. Lai, R. Parveen, C. M. Donahue, M. M. Wymore, B. A. Massman, B. Vlaisavljevich, T. S. Teets and S. R. Daly, Modifying the luminescent properties of a Cu(I) diphosphine complex using ligand-centered reactions in single crystals, *Chem. Commun.*, 2020, **56**, 9110–9113.
31 V. A. Krylova, P. I. Djurovich, M. T. Whited and M. E. Thompson, Synthesis and characterization of phosphorescent three-coordinate Cu(I)–NHC complexes, *Chem. Commun.*, 2010, **46**, 6696–6698.
32 V. A. Krylova, P. I. Djurovich, J. W. Aronson, R. Haiges, M. T. Whited and M. E. Thompson, Structural and Photophysical Studies of Phosphorescent Three-Coordinate Copper(I) Complexes Supported by an N-Heterocyclic Carbene Ligand, *Organometallics*, 2012, **31**, 7983–7993.
33 V. A. Krylova, P. I. Djurovich, B. L. Conley, R. Haiges, M. T. Whited, T. J. Williams and E. Mark, Thompson, Control of emission colour with N-heterocyclic carbene (NHC) ligands in phosphorescent three-coordinate Cu(I) complexes, *Chem. Commun.*, 2014, **50**, 7176–7179.
34 M. Elie, F. Sguerra, F. D. Meo, M. D. Weber, R. Marion, A. Grimault, J.-F. Lohier, A. Stallivieri, A. Brosseau, R. B. Pansu, J.-L. Renaud, M. Linares, M. Hamel, R. D. Costa and S. Gaillard, Designing NHC–Copper(I) Dipyridylamine Complexes for Blue Light-Emitting Electrochemical Cells, *ACS Appl. Mater. Interfaces*, 2016, **8**, 14678–14691.
35 M. Elie, M. D. Weber, F. Di Meo, F. Sguerra, J.-F. Lohier, R. B. Pansu, J.-L. Renaud, M. Hamel, M. Linares, R. D. Costa and S. Gaillard, Role of the Bridging Group in Bis-Pyridyl Ligands: Enhancing Both the Photo- and Electroluminescent Features of Cationic (IPr)CuI, Complexes, *Chem. – Eur. J.*, 2017, **23**, 16328–16337.
36 K. Glinton, R. Latifi, D. S. Cockrell, M. Bardeaux, B. Nguyen and L. Tahsini, Synthesis, characterization, and photo-luminescent studies of three-coordinate Cu(I)–NHC complexes bearing unsymmetrically-substituted dipyridyl-amine ligands, *RSC Adv.*, 2019, **9**, 22417–22427.
37 M. J. Leitl, V. A. Krylova, P. I. Djurovich, M. E. Thompson and H. Yersin, Phosphorescence versus Thermally Activated Delayed Fluorescence. Controlling Singlet–Triplet Splitting in Brightly Emitting and Sublimable Cu(I) Compounds, *J. Am. Chem. Soc.*, 2014, **136**, 16032–16038.
38 B. Hupp, C. Schiller, C. Lenczyk, M. Stanoppi, K. Edkins, A. Lorbach and A. Steffen, Synthesis, Structures, and Photophysical Properties of a Series of Rare Near-IR Emitting Copper(I) Complexes, *Inorg. Chem.*, 2017, **56**, 8996–9008.
39 R. Marion, F. Sguerra, F. D. Meo, E. Sauvageot, J.-F. Lohier, R. Daniellou, J.-L. Renaud, M. Linares, M. Hamel and S. Gaillard, NHC Copper(I) Complexes Bearing Dipyridylamine Ligands: Synthesis, Structural, and Photoluminescent Studies, *Inorg. Chem.*, 2014, **53**, 9181–9191.
40 S. Shi, P. I. Djurovich and M. E. Thompson, Synthesis and characterization of phosphorescent three-coordinate copper(I) complexes bearing bis(amino)cyclopropenylidene carbene (BAC), *Inorg. Chim. Acta*, 2018, **482**, 246–251.
41 R. Molteni, K. Edkins, M. Haehnel and A. Steffen, C–H Activation of Fluoroarenes: Synthesis, Structure, and Luminescence Properties of Copper(I) and Gold(I) Complexes Bearing 2-Phenylpyridine Ligands, *Organometallics*, 2016, **35**, 629–640.
42 A. S. Romanov, F. Chotard, J. Rashid and M. Bochmann, Synthesis of copper(I) cyclic (alkyl)(amino)carbene complexes with potentially bidentate N^N, N^S and S^S ligands

for efficient white photoluminescence, *Dalton Trans.*, 2019, **48**, 15445–15454.

43 D. Kim and T. S. Teets, Sterically Encumbered Aryl Isocyanides Extend Excited-State Lifetimes and Improve the Photocatalytic Performance of Three-Coordinate Copper(I) β-Diketiminate Charge-Transfer Chromophores, *J. Am. Chem. Soc.*, 2024, **146**, 16848–16855.

44 D. Kim, M. C. Rosko, F. N. Castellano, T. G. Gray and T. S. Teets, Long Excited-State Lifetimes in Three-Coordinate Copper(I) Complexes via Triplet–Triplet Energy Transfer to Pyrene-Decorated Isocyanides, *J. Am. Chem. Soc.*, 2024, **146**, 19193–19204.

45 A. Kumar, D. Kim, G. Nguyen, C. Jiang, S. Chakraborty and T. S. Teets, Photophysical properties of three-coordinate heteroleptic Cu(I) β-diketiminate triarylphosphine complexes, *Dalton Trans.*, 2025, **54**, 396–404.

46 H. Dolati, L. Denker, B. Trzaskowski and R. Frank, Superseding β-Diketiminato Ligands: An Amido Imidazoline-2-Imine Ligand Stabilizes the Exhaustive Series of B = X Boranes (X = O, S, Se, Te), *Angew. Chem., Int. Ed.*, 2021, **60**, 4633–4639.

47 H. Dolati, L. Denker, J. P. Martínez, B. Trzaskowski and R. Frank, Iminoboranes With Parent B = NH Entity: Imino Group Metathesis, Nucleophilic Reactivity and N–N Coupling, *Chem. – Eur. J.*, 2023, **29**, e202302494.

48 X. Wu and M. Tamm, Transition metal complexes supported by highly basic imidazolin-2-iminato and imidazolin-2-imine N-donor ligands, *Coord. Chem. Rev.*, 2014, **260**, 116–138.

49 M. Tamm, D. Petrovic, S. Randoll, S. Beer, T. Bannenberg, P. G. Jones and J. Grunenberg, Structural and theoretical investigation of 2-iminoimidazolines – carbene analogues of iminophosphoranes, *Org. Biomol. Chem.*, 2007, **5**, 523–530.

50 D. Petrovic, T. Bannenberg, S. Randoll, P. G. Jones and M. Tamm, Synthesis and reactivity of copper(I) complexes containing a bis(imidazolin-2-imine) pincer ligand, *Dalton Trans.*, 2007, 2812–2822.

51 D. Petrovic, T. Glöge, T. Bannenberg, C. G. Hrib, S. Randoll, P. G. Jones and M. Tamm, Synthesis and Reactivity of 16-Electron Pentamethylcyclopentadienyl–Ruthenium(II) Complexes with Bis(imidazolin-2-imine) Ligands, *Eur. J. Inorg. Chem.*, 2007, 3472–3475.

52 D. Petrovic, L. M. R. Hill, P. G. Jones, W. B. Tolman and M. Tamm, Synthesis and reactivity of copper(I) complexes with an ethylene-bridged bis(imidazolin-2-imine) ligand, *Dalton Trans.*, 2008, 887–894.

53 D. Petrovic, C. G. Hrib, S. Randoll, P. G. Jones and M. Tamm, Synthesis and Reactivity of 16-Electron Cycloheptatrienyl-Molybdenum(0) Complexes with Bis(imidazolin-2-imine) Ligands, *Organometallics*, 2008, **27**, 778–783.

54 T. K. Panda, C. G. Hrib, P. G. Jones, J. Jenter, P. W. Roesky and M. Tamm, Rare Earth and Alkaline Earth Metal Complexes with Me_2Si-Bridged Cyclopentadienyl-Imidazolin-2-Imine Ligands and Their Use as Constrained-Geometry Hydroamination Catalysts, *Eur. J. Inorg. Chem.*, 2008, 4270–4279.

55 T. Glöge, D. Petrovic, C. G. Hrib, P. G. Jones and M. Tamm, 16-Electron (Arene)ruthenium Complexes with Superbasic Bis(imidazolin-2-imine) Ligands and Their Use in Catalytic Transfer Hydrogenation, *Eur. J. Inorg. Chem.*, 2009, 4538–4546.

56 T. Glöge, D. Petrovic, C. G. Hrib, C. Daniliuc, E. Herdtweck, P. G. Jones and M. Tamm, Synthesis and Structural Characterisation of an Isomorphous Series of Bis(imidazolin-2-imine) Metal Dichlorides Containing the First Row Transition Metals Mn, Fe, Co, Ni, Cu and Zn, *Z. Anorg. Allg. Chem.*, 2010, **636**, 2303–2308.

57 J. Bogojeski, R. Jelić, D. Petrović, E. Herdtweck, P. G. Jones, M. Tamm and Ž. D. Bugarčić, Equilibrium studies of the reactions of palladium(II) bis(imidazolin-2-imine) complexes with biologically relevant nucleophiles. The crystal structures of $[(TL^{tBu})PdCl]ClO_4$ and $[(BL^{iPr})PdCl_2]$, *Dalton Trans.*, 2011, **40**, 6515–6523.

58 S.-A. Filimon, D. Petrovic, J. Volbeda, T. Bannenberg, P. G. Jones, C.-G. Freiherr von Richthofen, T. Glaser and M. Tamm, 3d Metal Complexes Supported by a Bis(imidazolin-2-imino)pyridine Pincer Ligand – Synthesis, Structural Characterisation, and Magnetic Properties, *Eur. J. Inorg. Chem.*, 2014, 5997–6012.

59 T. Glöge, K. Jess, T. Bannenberg, P. G. Jones, N. Langenscheidt-Dabringhausen, A. Salzer and M. Tamm, 16-Electron pentadienyl- and cyclopentadienyl-ruthenium half-sandwich complexes with bis(imidazol-2-imine) ligands and their use in catalytic transfer hydrogenation, *Dalton Trans.*, 2015, **44**, 11717–11724.

60 T. Glöge, F. Aal, S.-A. Filimon, P. G. Jones, J. Michaelis de Vasconcellos, S. Herres-Pawlis and M. Tamm, Transition Metal Complexes Containing C_2-Symmetric Bis(imidazolin-2-imine) Ligands Derived from a 1-Alkyl-3-arylimidazolin-2-ylidene, *Z. Anorg. Allg. Chem.*, 2015, **641**, 2204–2214.

61 J. Bogojeski, J. Volbeda, M. Freytag, M. Tamm and Ž. D. Bugarčić, Palladium(II) complexes with highly basic imidazolin-2-imines and their reactivity toward small biomolecules, *Dalton Trans.*, 2015, **44**, 17346–17359.

62 K. Jess, D. Baabe, T. Bannenberg, K. Brandhorst, M. Freytag, P. G. Jones and M. Tamm, Ni–Fe and Pd–Fe Interactions in Nickel(II) and Palladium(II) Complexes of a Ferrocene-Bridged Bis(imidazolin-2-imine) Ligand, *Inorg. Chem.*, 2015, **54**, 12032–12045.

63 L. Denker, B. Trzaskowski and R. Frank, "Give me five" – an amino imidazoline-2-imine ligand stabilises the first neutral five-membered cyclic triel(I) carbenoides, *Chem. Commun.*, 2021, **57**, 2816–2819.

64 L. Denker, H. Dolati, M. Barthen and R. Frank, Amino Imidazolin-2-imine Ligands in Magnesium Complexes: Approaches Towards Low-Valent Mg(I) Species, *Z. Anorg. Allg. Chem.*, 2024, **650**, e202300247.

65 L. Denker, D. Wullschläger, J. P. Martínez, S. Swierczewski, B. Trzaskowski, M. Tamm and R. Frank, Cobalt(I)-Catalyzed Transformation of Si–H Bonds: H/D Exchange in Hydrosilanes and Hydrosilylation of Olefins, *ACS Catal.*, 2023, **13**, 2586–2600.

66 N. U. D. Reshi, D. Bockfeld, D. Baabe, L. Denker, J. P. Martínez, B. Trzaskowski, R. Frank and M. Tamm, Iron (I) and Iron(II) Amido-imidazolin-2-imine Complexes as Catalysts for H/D Exchange in Hydrosilanes, *ACS Catal.*, 2024, **14**, 1759–1772.
67 A. Cotton, X. Feng, M. Matusz and R. Poli, Experimental and Theoretical Studies of the Copper(I) and Silver(I) Dinuclear *N,N*(-Di-*p*-tolylformamidinaato Complexes, *J. Am. Chem. Soc.*, 1988, **110**, 7077–7083.
68 B. S. Lim, A. Rahtu, J.-S. Park and R. G. Gordon, Synthesis and Characterization of Volatile, Thermally Stable, Reactive Transition Metal Amidinates, *Inorg. Chem.*, 2003, **42**, 7951–7958.
69 A. C. Lane, M. V. Vollmer, C. H. Laber, D. Y. Melgarejo, G. M. Chiarella, J. P. Fackler, X. Yang, G. A. Baker and J. R. Walensky, Multinuclear Copper(I) and Silver(I) Amidinate Complexes: Synthesis, Luminescence, and CS_2 Insertion Reactivity, *Inorg. Chem.*, 2014, **53**, 11357–11366.
70 X. Jiang, J. C. Bollinger, M.-H. Baik and D. Lee, Copper clusters built on bulky amidinate ligands: spin delocalization via superexchange rather than direct metal–metal bonding, *Chem. Commun.*, 2005, 1043–1045.
71 C. Jones, C. Schulten, L. Fohlmeister, A. Stasch, K. S. Murray, B. Moubaraki, S. Kohl, M. Z. Ertem, L. Gagliardi and C. J. Cramer, Bulky Guanidinato Nickel(I) Complexes: Synthesis, Characterization, Isomerization, and Reactivity Studies, *Chem. – Eur. J.*, 2011, **17**, 1294–1303.
72 A. M. Willcocks, T. P. Robinson, C. Roche, T. Pugh, S. P. Richards, A. J. Kingsley, J. P. Lowe and A. L. Johnson, Multinuclear Copper(I) Guanidinate Complexes, *Inorg. Chem.*, 2012, **51**, 246–257; X. Dai and T. H. Warren, Discrete Bridging and Terminal Copper Carbenes in Copper-Catalyzed Cyclopropanation, *J. Am. Chem. Soc.*, 2004, **126**, 10085–10094.
73 Y. M. Badiei, A. Dinescu, X. Dai, R. M. Palomino, F. W. Heinemann, T. R. Cundari and T. H. Warren, Copper–Nitrene Complexes in Catalytic C-H Amination, *Angew. Chem., Int. Ed.*, 2008, **47**, 9961–9964.
74 X. Dai and T. H. Warren, Dioxygen activation by a neutral β-diketiminato copper(I) ethylene complex, *Chem. Commun.*, 2001, 1998–1999.
75 C. Shimokawa, S. Yokota, Y. Tachi, N. Nishiwaki, M. Ariga and S. Itoh, Substituent Effects of *β*-Diketiminate Ligands on the Structure and Physicochemical Properties of Copper (II) Complexes, *Inorg. Chem.*, 2003, **42**, 8395–8405.
76 D. Kim, T. G. Gray and T. S. Teets, Heteroleptic copper(I) charge-transfer chromophores with panchromatic absorption, *Chem. Commun.*, 2022, **58**, 11446–11449.
77 R. C. Holz and J. M. Brink, Proton NMR Spectroscopy as a Probe of Dinuclear Copper(II) Centers, *Inorg. Chem.*, 1994, **33**, 4609–4610.
78 N. N. Murthy, D. D. Karlin, I. Bertini and C. Luchinat, NMR and electronic relaxation in paramagnetic Dicopper(II) compounds, *J. Am. Chem. Soc.*, 1997, **119**, 2156–2162.
79 L. Banci, I. Bertini and C. Luchinat, The ^{1}H NMR parameters of magnetically coupled dimers – The Fe_2S_2 proteins as an example, *Struct. Bonding*, 1990, **72**, 113–135.
80 I. A. Koval, K. van der Schilden, A. M. Schuitema, P. Gamez, C. Belle, J.-L. Pierre, M. Lüken, B. Krebs, O. Roubeau and J. Reedijk, Proton NMR Spectroscopy and Magnetic Properties of a Solution-Stable Dicopper(II) Complex Bearing a Single *μ*-Hydroxo Bridge, *Inorg. Chem.*, 2005, **44**, 4372–4382.
81 G. De Munno, D. Viterbo, A. Caneschi, F. Lloret and M. Julve, A Giant Antiferromagnetic Interaction through the Bihydroxide Bridge, *Inorg. Chem.*, 1994, **33**, 1585–1586.
82 D. Kim, M. C. Rosko, V. Q. Dang, F. N. Castellano and T. S. Teets, Sterically Encumbered Heteroleptic Copper(I) *β*-Diketiminate Complexes with Extended Excited-State Lifetimes, *Inorg. Chem.*, 2023, **62**, 16759–16769.
83 D. Kim and T. S. Teets, A series of four-coordinate heteroleptic copper(I) complexes with diimine and β-diketiminate ligands, *Polyhedron*, 2024, **248**, 116748.
84 R. Czerwieniec, M. J. Leitl, H. H. H. Homeier and H. Yersin, Cu(I) complexes – Thermally activated delayed fluorescence. Photophysical approach and material design, *Coord. Chem. Rev.*, 2016, **15**, 2–28.
85 N. Haase, A. Danos, C. Pflumm, A. Morherr, P. Stachelek, A. Mekic, W. Brütting and A. Monkman, Kinetic Modeling of Transient Photoluminescence from Thermally Activated Delayed Fluorescence, *J. Phys. Chem. C*, 2018, **122**, 29173–29179.
86 J. Eng and T. Penfold, Understanding and Designing Thermally Activated Delayed Fluorescence Emitters: Beyond the Energy Gap Approximation, *Chem. Rec.*, 2020, **20**, 831–856.
87 T. Hofbeck, U. Monkowius and H. Yersin, Highly Efficient Luminescence of Cu(I) Compounds: Thermally Activated Delayed Fluorescence Combined with Short-Lived Phosphorescence, *J. Am. Chem. Soc.*, 2015, **137**, 399–404.
88 S. Chakraborty, K. Agyekum, D. Kim and T. S. Teets, Ligand substituents modulate excited-state lifetime and energy-transfer reactivity in Cu(i) photosensitizers supported by salicylaldimine and isocyanide ligands, *Chem. Sci.*, 2025, Advance Article, DOI: **10.1039/d5sc07286g**.
89 (*a*) CCDC 2428671: Experimental Crystal Structure Determination, 2025, DOI: **10.5517/ccdc.csd.cc2mj77n**; (*b*) CCDC 2428672: Experimental Crystal Structure Determination, 2025, DOI: **10.5517/ccdc.csd.cc2mj78p**; (*c*) CCDC 2428673: Experimental Crystal Structure Determination, 2025, DOI: **10.5517/ccdc.csd.cc2mj79q**; (*d*) CCDC 2428674: Experimental Crystal Structure Determination, 2025, DOI: **10.5517/ccdc.csd.cc2mj7br**; (*e*) CCDC 2428675: Experimental Crystal Structure Determination, 2025, DOI: **10.5517/ccdc.csd.cc2mj7cs**; (*f*) CCDC 2428676: Experimental Crystal Structure Determination, 2025, DOI: **10.5517/ccdc.csd.cc2mj7dt**; (*g*) CCDC 2428677: Experimental Crystal Structure Determination, 2025, DOI: **10.5517/ccdc.csd.cc2mj7fv**; (*h*) CCDC 2428678: Experimental Crystal Structure Determination, 2025, DOI: **10.5517/ccdc.csd.cc2mj7gw**; (*i*) CCDC 2428679: Experimental Crystal Structure Determination, 2025, DOI: **10.5517/ccdc.csd.cc2mj7hx**; (*j*) CCDC 2428680: Experimental Crystal Structure Determination, 2025, DOI: **10.5517/ccdc.csd.cc2mj7jy**.

